



HAL
open science

Wheat canopy structure and surface roughness effects on multiangle observations at L-Band

S. Peischl, J.P. Walker, D. Ryu, Yann H. Kerr, R. Panciera, C. Rüdiger

► **To cite this version:**

S. Peischl, J.P. Walker, D. Ryu, Yann H. Kerr, R. Panciera, et al.. Wheat canopy structure and surface roughness effects on multiangle observations at L-Band. *IEEE Transactions on Geoscience and Remote Sensing*, 2012, 50 (5), pp.1498-1506. 10.1109/TGRS.2011.2174644 . ird-00701154

HAL Id: ird-00701154

<https://ird.hal.science/ird-00701154>

Submitted on 24 May 2012

HAL is a multi-disciplinary open access archive for the deposit and dissemination of scientific research documents, whether they are published or not. The documents may come from teaching and research institutions in France or abroad, or from public or private research centers.

L'archive ouverte pluridisciplinaire **HAL**, est destinée au dépôt et à la diffusion de documents scientifiques de niveau recherche, publiés ou non, émanant des établissements d'enseignement et de recherche français ou étrangers, des laboratoires publics ou privés.



Wheat canopy structure and surface roughness effects on multi-angle observations at L-band

Journal:	<i>Transactions on Geoscience and Remote Sensing</i>
Manuscript ID:	Draft
Manuscript Type:	Soil Moisture and Ocean Salinity Mission 2010 Special Issue paper
Keywords:	Remote sensing, Microwave radiometry

SCHOLARONE™
Manuscripts

Review

1
2
3
4 1
5
6 2
7
8
9 3
10
11 4
12
13 5
14
15 6
16
17
18 7
19
20 8
21 9
22 10
23
24 11
25
26 12
27 13
28
29 14
30
31 15
32 16
33
34 17
35
36 18
37 19
38
39 20
40
41
42
43
44
45
46
47
48
49
50
51
52
53
54
55
56
57
58
59
60

Wheat canopy structure and surface roughness effects on multi-angle observations at L-band

Sandy Peischl, *Member, IEEE*, Jeffrey P. Walker, Dongryeol Ryu, *Member, IEEE*, Yann Kerr, *Senior Member, IEEE*, Rocco Panciera, Christoph Rüdiger, *Member, IEEE*

Contact details:

Sandy Peischl

Department of Civil Engineering
Building 60, Room 156, Clayton
Monash University Victoria 3800
Australia

Phone: +61 3 990 54957

Fax: +61 3 990 54944

E-mail: sandy.peischl@monash.edu

1
2
3
4 21
5 22 **Abstract**—The capability of multi-angle observations of the Soil moisture and Ocean Salinity
6
7 23 (SMOS) mission is expected to significantly improve the inversion of soil microwave emissions
8
9 24 for soil moisture by enabling the simultaneous retrieval of the vegetation optical depth and other
10
11 25 surface parameters. Consequently, this paper investigates the relationship between soil moisture
12
13 26 and brightness temperature at multiple incidence angles using airborne L-band data from the
14
15 27 National Airborne Field Experiment (NAFE) in Australia in 2005. A forward radio brightness
16
17 28 model was used to predict the passive microwave response at a range of incidence angles, given
18
19 29 inputs of i) ground measured soil and vegetation properties and ii) default model parameters for
20
21 30 vegetation and roughness characterization. Simulations were made across various dates and
22
23 31 locations with wheat cover and evaluated against the available airborne observations. The
24
25 32 comparison showed a significant underestimation of the measured brightness temperatures by the
26
27 33 model, when using the default parameterization. This discrepancy subsequently led to a soil
28
29 34 moisture retrieval error of up to $0.3 \text{ m}^3\text{m}^{-3}$. The analysis found that i) the roughness value H_r was
30
31 35 too low, which was then adjusted as a function of the soil moisture; while ii) the vegetation
32
33 36 structure parameters tt_h and tt_v were reduced by calibrating them from a single flight and testing
34
35 37 them for different moisture conditions and locations. The simulation error between the forward
36
37 38 model predictions and the airborne observations was improved from $\text{rmse}=31.3 \text{ K}$ (26.5 K) to
38
39 39 $\text{rmse}=2.3 \text{ K}$ (5.3 K) for wet and (dry) soil moisture conditions, respectively.
40
41
42
43
44
45
46
47
48
49

50 41 **Index Terms**—L-band Microwave Emission of the Biosphere (L-MEB), National Airborne
51
52 42 Field Experiment (NAFE), Microwave radiometry, Multi-angle, Remote Sensing, Soil Moisture
53
54 43 and Ocean Salinity (SMOS)
55
56
57
58
59
60

I. INTRODUCTION

The potential of passive microwave systems to monitor surface soil moisture has been extensively studied during the past decades [1]-[7] and are considered as one of the most relevant techniques. Microwave remote sensing is in particular suitable due to i) its high sensitivity to the dielectric properties of the soil-water medium, which can be directly related to the water content, ii) the reduced interference with the atmosphere and surface roughness, iii) the low attenuation effects of the vegetation layer and iv) its all-weather capability. Moreover, at low frequencies the penetration depth within the soil column is significant compared to other wavelengths. Hence, especially the protected L-band (~1-2 GHz) with a penetration depth of typically ~5 cm and low sensitivity to canopy and surface roughness is preferred for the purpose of soil moisture remote sensing. Consequently, the strong scientific demand for large scale L-band observations of soil moisture data, with a sufficient temporal resolution for application in hydrological, meteorological and agronomical disciplines [8], led to the first spaceborne mission specifically dedicated to the monitoring of soil moisture.

The Soil Moisture and Ocean Salinity (SMOS) satellite was launched in November 2009 by the European Space Agency (ESA) and designed to provide global maps of the surface soil moisture fields with an accuracy better than $0.04 \text{ m}^3 \text{ m}^{-3}$ for the nominal case of bare or low vegetated soils (non-nominal cases include mountainous and urban areas, frozen or very dry soils, ice and significant snow covered surfaces) [9],[10]. Importantly, the satellite's new antenna concept utilizes a 2-dimensional interferometric L-band radiometer to overcome the constraints given by the proportional relation between the antenna diameter and the resulting spatial resolution and hence achieves the desired pixel size of less than 50 km. Moreover one of the innovative features of SMOS is its capability of multi-incidence angle observations, that are

1
2
3
4 67 obtained by the along-track movement of the satellite and the corresponding quasi-simultaneous
5
6 68 acquisition of a series of brightness temperatures for a range of angles over the same location on
7
8 69 earth. Previous studies [11]-[13] have shown that there are significant angular signatures on the
9
10 70 measured radiometer signal associated with various land surface features and that in some cases
11
12 71 it is difficult to separate the contribution of the vegetation from the actual soil emission based on
13
14 72 single angle measurements. Thus, by understanding these angular dependencies, it has been
15
16 73 suggested that model parameters such as vegetation attenuation and surface roughness may be
17
18 74 simultaneously estimated, resulting in an enhanced and presumably more accurate soil moisture
19
20 75 retrieval [14]. Due to the absence of comparable spaceborne observations regarding the novel
21
22 76 SMOS configuration, retrieval algorithms such as L-MEB (L-band and Microwave Emission of
23
24 77 the Biosphere [15]) have been primarily tested and developed using synthetic simulations [16]
25
26 78 and small scale field experiments (SMOSREX [17], MELBEX [18] and EuroSTARRS [19]),
27
28 79 with the modeling of incidence angle relationships based on only a subset of the possible land
29
30 80 cover types. Consequently, the derived relationships and the model interactions between land
31
32 81 surface variables and observed brightness temperature response need to be verified at larger
33
34 82 spatial scales and extended for a wider range of land surface conditions.

35
36
37
38
39
40
41 83 The objective of this paper is to compare multi-angle L-band data from airborne observations
42
43 84 with simulated brightness temperatures using the L-MEB model and ground truth data as input.
44
45 85 Subsequently, the performance of the forward model parameterization is evaluated based on
46
47 86 different soil moisture conditions and locations and additional parameterizations are tested, that
48
49 87 included i) modifications of the modeled roughness and vegetation structure characterization.
50
51
52
53
54
55
56
57
58
59
60

88

89 II. EXPERIMENTAL DATA SET

90 The multi-incidence angle airborne data used in this paper were acquired in November 2005
91 during the National Airborne Field Experiment (NAFE'05) in south-east Australia. The
92 campaign was conducted over a period of four weeks including a combination of airborne
93 observations and ground measurements. A complete description of the experiment and the data
94 collection strategy is provided in [20], so only the pertinent details are summarized here.

95 A. Study Area

96 The field experiment concentrated on the northern part of the Goulburn River catchment (32°
97 S, 150° E) located in New South Wales, Australia. The 40 km × 40 km study region had been
98 subdivided into two main focus areas within the Merriwa River and Krui River catchment.
99 Across each of these two focus areas several smaller sites had been selected for intensive
100 airborne and ground operations at farm-scale. The multi-incidence angle flights, which are the
101 emphasis of this study, covered only three out of a total of eight focus farms including
102 Midlothian, Merriwa Park and Cullingral (Fig. 1). The observed terrain is fairly flat, with soil
103 types ranging from clay loams to sandy soils [21]. The regional climate can be described as sub-
104 humid and temperate with an average annual rainfall of 700 mm and a mean maximum annual
105 temperature of 30°C in summer and 16°C in winter. During the campaign period the focus farms
106 were dominated by grazing lands with native grass cover and cropping land use (mainly wheat,
107 barley and lucerne).

108 B. Airborne multi-angle Data

109 The primary airborne instrument used in the NAFE'05 campaign was the Polarimetric L-band
110 Multi-beam Radiometer (PLMR), which operates at a frequency of 1.413 GHz with a bandwidth
111 of 24 MHz. During the field experiment the L-band radiometer was typically used to measure

1
2
3 112 dual-polarized brightness temperatures in pushbroom mode at six viewing angles ($\pm 7^\circ$, $\pm 21.5^\circ$,
4
5 113 $\pm 37.5^\circ$). However, regarding the multi-angle data collection, PLMR was mounted on the aircraft
6
7
8 114 in an along-track configuration, resulting in three PLMR beams pointing forward and three
9
10 115 backward with respect to the flight direction of the aircraft. Consequently, as the aircraft moved
11
12 116 along its flight path, this setup provided a minimum of six quasi-simultaneous multi-incidence
13
14 117 angle observations of the same location on earth with a 17° (3-dB) antenna beamwidth. The
15
16 118 nominal flight altitude was about 750 m which corresponds to a spatial resolution of
17
18 119 approximately 250 m. In general, an area of $1.5 \text{ km} \times 6 \text{ km}$ was covered by four to five parallel
19
20 120 South-North oriented flight lines at each of the three farms. Dual-polarized multi-angle data were
21
22 121 acquired on four days (once a week) at Merriwa Park, and one day each for Midlothian and
23
24 122 Cullingral, respectively. Additionally, specific dive flights (i.e. successive steep
25
26 123 ascents/descents) were conducted immediately following the multi-angle flights over the focus
27
28 124 farms in order to provide observations with an even wider range of incidence angles ($\sim 3\text{-}60^\circ$).

29
30
31
32
33
34 125 Calibration of the PLMR instrument was carried out on a daily basis before and after the flight
35
36 126 using both the sky (cold calibration) and a blackbody box (warm calibration) as target.
37
38 127 Supplementary in-flight calibration checks were made through flights over a large water body
39
40 128 that was continuously monitored in terms of surface water temperature and salinity. A detailed
41
42 129 description of the complete calibration procedures can be found in [20]. Considering the range of
43
44 130 brightness temperature measurements over land during the campaign (150-300 K), the PLMR
45
46 131 accuracy was estimated by [20] to be higher than 0.7 K for H-polarization and 2 K for V-
47
48 132 polarization. The calibrated radiometer observations have further been processed to provide local
49
50 133 incidence angle and effective footprint size information taking into account ground topography,
51
52 134 aircraft position and attitude. Finally, the data were filtered to eliminate large aircraft yaw and
53
54
55
56
57
58
59
60

1
2
3 135 roll angles due to turbulences and wind forces. As a result, sun glint effects in the external beams
4
5
6 136 were also reduced.
7

8 9 137 *C. Ground Data*

10
11 138 Extensive ground sampling activities were conducted coincident with the airborne
12
13 139 observations, focusing on an area of approximately 1.5 km × 3.0 km at each farm (see Fig. 1).
14
15 140 The measurements of near-surface soil moisture (0-5 cm) were made using the Hydraprobe Data
16
17 141 Acquisition System (HDAS, [22]), which consists of a Hydraprobe soil moisture sensor, a Global
18
19 142 Positioning System (GPS) and a handheld pocket PC that has a Geographic Information System
20
21 143 (GIS) installed to provide a visual output of the sampling location and the corresponding soil
22
23 144 moisture observation. The HDAS measurements were made over a spatial sampling grid with
24
25 145 varying spacing from 6.25 m to 2 km. The high-resolution sampling (6.25 m - 12.5 m) was
26
27 146 mainly concentrated on an area of 150 m × 150 m within the cropping fields at Merriwa Park and
28
29 147 Cullingral and within a large patch of native grass at Midlothian. The surrounding areas were
30
31 148 sampled at coarser spatial scales. The Hydraprobe standard soil moisture product was calibrated
32
33 149 against gravimetric soil samples from the field and laboratory data and corrected for temperature
34
35 150 effects, resulting in an estimated accuracy of $\pm 0.033 \text{ m}^3 \text{ m}^{-3}$ [22]. The gravimetric samples were
36
37 151 further analyzed in terms of soil texture and soil properties (Table I). Supplementary data
38
39 152 including land use, surface roughness, rock cover fraction, rock temperature, dew amount,
40
41 153 vegetation biomass and vegetation water content were also recorded at each farm site. Climate
42
43 154 data were available through an existing in-situ monitoring network
44
45 155 (www.eng.newcastle.edu.au/sasmas/SASMAS/sasmas.htm) collecting long-term soil moisture
46
47 156 (0-5 cm, 0-30 cm, 30-60 cm and 60-90 cm), soil temperature (0-5 cm and 0-30 cm) and rainfall
48
49 157 data. During the campaign a few stations were temporarily upgraded with additional
50
51
52
53
54
55
56
57
58
59
60

1
2
3 158 instrumentation including thermal infrared sensors (TIR), surface soil-temperature profiles (1
4
5 159 cm, 2.5 cm and 4 cm) and leaf wetness sensors to determine the presence of dew. Midlothian,
6
7
8 160 Merriwa Park and Cullingral were each equipped with one permanent and one temporary
9
10 161 monitoring station. The latter was always located within the high-resolution soil moisture
11
12 162 sampling area of the focus farm.

13
14
15 163 This paper focuses on the use of multi-incidence angle airborne observations and ground data
16
17 164 collected across the cropping fields at Merriwa Park and Cullingral. Both sites were covered by
18
19 165 mature wheat, whereas Midlothian was predominantly characterized by native grass and lucerne.
20
21 166 Consequently, data collected across the Midlothian site was not considered in this study. Table I
22
23 167 summarizes the main features of the Merriwa Park and Cullingral study sites showing an overall
24
25 168 dynamic soil moisture range of about 0.05-0.55 m³m⁻³ for Merriwa Park over the entire period.
26
27 169 Moist soil conditions were generally observed at the start of the campaign in response to
28
29 170 significant rainfall in the area, while towards the end of the field experiment the topsoil showed
30
31 171 substantial drying effects. Cullingral was only covered once with multi-angle flights and
32
33 172 corresponding in-situ soil moisture measurements during the campaign. The spatial soil moisture
34
35 173 distribution across Cullingral ranged from 0.05-0.25 m³m⁻³ on the observation day.
36
37
38
39
40
41

42 174 III. RADIATIVE TRANSFER MODEL

43
44
45 175 The radiative transfer model used in this study is the L-band Microwave Emission of the
46
47 176 Biosphere (L-MEB) model [15], which is the core element of the operational soil moisture
48
49 177 retrieval algorithm developed for SMOS [23]. A detailed description of the model structure and
50
51 178 parameterization is presented in [15], so the following discussion concentrates only on the basic
52
53 179 principles of L-MEB.
54
55

56
57 180 The presence of vegetation and the resulting interaction with the soil surface emission are
58
59
60

1
2
3 181 described in terms of a simplified (zero-order) solution of the radiative transfer approach, also
4
5 182 known as the tau-omega model. This algorithm assumes that the influence of the vegetation layer
6
7
8 183 on the p -polarized soil reflectivity (r_{GP}) is accounted for by vegetation attenuation (Y_p) and
9
10 184 scattering effects (ω) and results in a composite brightness temperature (TB_p) as follows:
11
12

13 185
14
15 186
$$TB_p = (1 - \omega_p)(1 - Y_p)(1 + Y_p r_{GP})T_C + (1 - r_{GP})Y_p T_G, \quad (1)$$

16
17

18 187
19
20 188 where T_G and T_C correspond to the effective soil and vegetation temperature [K], respectively.
21

22 189 The reflectivity of the underlying soil surface (r_{GP}) is a function of the wave polarization, the
23
24 190 observation frequency and the incidence angle, and can be quantified for non-smooth surfaces by
25
26
27 191 calculating the smooth surface Fresnel reflectivity (r_{GP}^*) and adjusting it through the use of a set
28
29
30 192 of soil roughness parameters (i.e. H_r and N_{rp}):
31

32 193
33
34 194
$$r_{GP} = r_{GP}^* \cdot \exp[-H_r \cos(\theta)^{N_{rp}}]. \quad (2)$$

35
36
37 195

38
39 196 Note, that N_{rp} is introduced to parameterize the angular dependence of the surface roughness.
40

41 197 The attenuation effect caused by the canopy, also referred to as transmissivity, is expressed as a
42
43
44 198 function of the vegetation optical depth (τ_p) and the incidence angle (θ):
45
46
47 199

48
49 200
$$Y_p = \exp(-\tau_p / \cos(\theta)). \quad (3)$$

50
51
52 201

53
54 202 The optical depth in turn can be computed as a linear function of the vegetation water content
55
56 203 (VWC) and the empirical parameter b_p , which is mainly dependent on the sensor frequency,
57
58
59
60

1
2
3 204 polarization, canopy type and plant structure [24]:
4
5

6 205

7
8 206
$$\tau_{nad} = VWC \cdot b_p . \quad (4)$$

9

10 207

11
12
13 208 Since (4) is strictly valid for nadir observations ($\theta=0^\circ$), two additional specific vegetation
14
15 209 structure parameters tt_h , tt_v (h and v denoting horizontal and vertical polarization) are introduced
16
17 210 that account for the angular effect on the optical depth and hence on the vegetation
18
19 211 transmissivity:
20
21
22

23 212

24
25 213
$$\tau_p = \tau_{nad} (\sin^2(\theta) \cdot tt_p + \cos^2(\theta)) . \quad (5)$$

26
27

28 214

29
30 215 Considering a value of $tt_p > 1$ or $tt_p < 1$ results either in an increasing or decreasing trend of the
31
32 216 optical depth, respectively, as a function of the incidence angle. The particular case of $tt_v = tt_h = 1$
33
34 217 corresponds to the isotropic state, where the optical depth of the standing canopy is assumed to
35
36 218 be independent of both polarization and incidence angle.
37
38
39

40
41 219

IV. MODELING APPROACH AND PARAMETERIZATION

42

43 220 The L-MEB forward model was used to generate dual-polarized brightness temperatures at a
44
45 221 range of incidence angles and moisture conditions by implementing the NAFE'05 data described
46
47 222 in Section II. The model set up was based on two types of input parameters: i) default model
48
49 223 parameters as a function of the land cover class and ii) ground truth information collected at the
50
51 224 focus farms. The available ground data for the two focus farms Merriwa Park and Cullingral
52
53 225 included soil moisture, soil texture, bulk density, soil profile temperature, vegetation water
54
55
56
57
58
59
60

1
2
3 226 content and vegetation temperature data. The input soil moisture was calculated by averaging all
4
5 227 high-resolution, near-surface ground measurements falling within the same PLMR footprint for
6
7
8 228 each observation day. The total number of HDAS measurements was generally between ~250-
9
10 229 300 points per observation day and radiometer footprint. Further model input included a special
11
12 230 set of parameters for surface roughness and vegetation characterization, i.e. variables H_R and N_{RP}
13
14 231 for the soil layer and tt_P , ω_p and b_P for the wheat canopy. These values were sourced from the
15
16 232 study by [15], in which the parameters had been calibrated from the PORTOS-93 experiment
17
18 233 over wheat at the Avignon test site in France [25]. This parameterization proposed by [15] is
19
20 234 hereafter referred to as the ‘default’ parameter set. Using the ground data and the default
21
22 235 parameterization, brightness temperature estimates were calculated for both H- and V-
23
24 236 polarization and incidence angles ranging from 0-50°. The forward simulations were done for all
25
26 237 available dates at Merriwa Park and Cullingral with the L-MEB results compared against the
27
28 238 actual airborne multi-incidence angle observations of the corresponding day and test site. Further
29
30 239 to the default model simulations described above, two additional parameter sets were tested
31
32 240 based on modifications of the initial model parameterization (Table II). In the second forward
33
34 241 model approach the default parameterization was changed in terms of a single model parameter;
35
36 242 the soil roughness value H_R given in [15] was replaced by a soil moisture dependent roughness
37
38 243 value proposed by [26] for the same study site. The basis for using a soil roughness value as a
39
40 244 function of soil moisture is due to a phenomenon known as “dielectric roughness”, which
41
42 245 contributes to volume scattering of the signal coming from deeper soil layers, and is assumed to
43
44 246 be caused by a variation of dielectric properties within the soil column due to a non-uniform
45
46 247 distribution of the water particles at micro-scale [27],[28]. Thus, in addition to the spatial
47
48 248 variations in the surface height (“geometric roughness”), it has been postulated that the
49
50
51
52
53
54
55
56
57
58
59
60

1
2
3 249 “dielectric roughness” should also be accounted for in terms of an effective H_R parameter. The
4
5
6 250 study by [26] was based on high-resolution (62.5 m), single-angle PLMR data from the
7
8 251 NAFE’05 experiment and suggested that the default H_R value in L-MEB was too low for
9
10 252 vegetation with dominant vertical structure such as wheat and barley. Note that [29] also had to
11
12 253 increase the H_R parameter for their studies when they used airborne L-band data over the same
13
14 254 test site but acquired by the EMIRAD radiometer, suggesting that the higher roughness values
15
16 255 were not related to an instrument-specific bias of the PLMR instrument itself. Moreover, [26]
17
18 256 found that the on-site calibrated H_R value demonstrated a notable temporal variation which
19
20 257 correlated with the observed moisture conditions during the field experiment. These results were
21
22 258 consistent with those published by [30] over bare soil at the SMOSREX test site. Hence [26]
23
24 259 developed a simple linear relationship between H_R and the soil moisture content for the
25
26 260 NAFE’05 test sites, which estimated lower H_R values with increasing moisture content.
27
28 261 Considering these results, the second parameterization had been set to include a roughness value
29
30 262 specifically calculated for each observation date depending on the corresponding soil moisture
31
32 263 information of that day. Note that since this linear function is soil type-specific, the defined
33
34 264 relationship between roughness effects and soil moisture is different for Merriwa Park and
35
36 265 Cullingral, where the soil texture changes from silty clay loam to silty loam, respectively (see
37
38
39
40
41
42
43
44 266 Table I).

45
46 267 The third parameter set included two modifications compared to the default L-MEB
47
48 268 parameterization: i) H_R calculated as a function of the actual soil moisture content (as in the
49
50 269 second model approach) and ii) calibrated vegetation structure variables tt_h and tt_v using the
51
52 270 available multi-incidence data for one of the four observation days. These vegetation parameters
53
54
55 271 were estimated through an optimization routine which had been applied to a single flight day
56
57
58
59
60

1
2
3 272 over Merriwa Park (9 November 2005). The calibrated values for tt_h and tt_v corresponded,
4
5 273 respectively, to a decrease ($tt_h < 1$) and increase ($tt_v > 1$) of the optical depth with the incidence
6
7
8 274 angle at each polarization, which was expected due to the dominantly vertical structure of the
9
10 275 wheat canopy. This parameterization was then applied to all remaining observation days at
11
12 276 Merriwa Park to assess its performance. Subsequently, the calibrated model variables were
13
14
15 277 further tested on airborne data from Cullingral in order to study their robustness and to verify the
16
17 278 parameterization derived from the Merriwa Park study site. The assumption that the remaining
18
19 279 vegetation values as proposed by [15] for i) the vegetation parameter b and ii) the single
20
21 280 scattering albedo ω were representative was justified based on: i) a site-specific calibration
22
23 281 across the available observation dates that showed no significant variations from $b=0.08$ and ω
24
25 282 $=0$ and ii) the fact that the parameterization resulted from an extensive literature review by [15].
26
27 283 Further analysis of the three parameterizations included the inversion of the L-MEB model to
28
29 284 solve an optimization problem for the retrieval of soil moisture given *a priori* ground truth
30
31 285 information. The algorithm was based on a minimized cost function that calculated the quadratic
32
33 286 difference between the measured and simulated brightness temperatures.
34
35
36
37
38
39

40 287 V. RESULTS AND DISCUSSION

41
42 288 The comparison of the L-MEB predicted brightness temperature response with the airborne
43
44 289 multi-angle observations from Merriwa Park and Cullingral for incidence angles ranging from 0-
45
46 290 50° showed significant discrepancies depending on the model parameterization chosen (Fig. 2).
47
48 291 Using the default L-MEB parameterization, the forward model consistently underestimated the
49
50 292 multi-angle observations at H-polarization, whereas at V-polarization (especially for large
51
52 293 incidence angles and wet soil conditions) the simulated brightness temperatures were much
53
54
55 294 higher than those observed. Furthermore, the exhibited angular trends of the dual-polarized
56
57
58
59
60

1
2
3 295 observations were only partially captured by the simulation results. Hence, differences of up to
4
5
6 296 ~40 K in brightness temperatures were observed, particularly within the range of low angles.
7
8 297 While this difference decreased for the vertical polarized curve with larger incidence angles, the
9
10 298 simulated horizontal brightness temperatures were always lower than the measured data. Note,
11
12 299 that for wet conditions at Merriwa Park during the first two observation days, the simulated
13
14 300 horizontally polarized curve is relatively flat due to the high vegetation water content and the
15
16 301 corresponding large value for the optical depth. The explanation behind this trend is that both the
17
18 302 attenuation of the soil emission and the emission by the wheat canopy itself increased, causing
19
20 303 the effective composite brightness temperature of both media to be closer to the effective
21
22 304 temperature of the vegetation. So with larger incidence angles, the attenuation of the vegetation
23
24 305 increased with respect to the $1/\cos(\theta)$ relationship as shown in equation (3). Setting a default
25
26 306 value of 1 for tt_h further assumes that there are no significant angular dependencies across the
27
28 307 observed wheat canopy at H-polarization. The comparison of the predicted and observed
29
30 308 brightness temperatures across the four observation days at Merriwa Park produced a root mean
31
32 309 square error (rmse) ranging from 38 K to 26 K for wet and dry conditions, respectively (Fig. 3),
33
34 310 when using the default parameters.

311 The overall model performance was improved by introducing the soil moisture dependent
312 roughness value H_r (second model parameterization) from the site-specific calibration presented
313 by [26]. Consequently, an upward translation of the modelled brightness temperature curves was
314 achieved resulting in a closer agreement with the actual observations. The corresponding root
315 mean square errors ranged between 9.6 K (wet) to 2.9 K (dry), and were thus significantly
316 reduced compared to the default model parameterization output. However, the simulated angular
317 behaviour was still unable to capture the observed brightness temperature trend exhibited at large

1
2
3 318 angles ($> 25^\circ$), which was especially dominant for moist conditions at Merriwa Park at the start
4
5 319 of the campaign. Moreover, for relatively low moisture contents ($< 0.1 \text{ m}^3\text{m}^{-3}$) the curve shift
6
7
8 320 forced by the moisture adjusted roughness value towards higher brightness temperatures was too
9
10
11 321 strong. Hence, the predicted emissions tended to overestimate the brightness temperature
12
13 322 measurements especially for dry conditions. A site-specific calibration of H_r based on the multi-
14
15 323 angle observations available for Merriwa Park (not shown in this paper) confirmed a non-linear
16
17
18 324 relationship between soil moisture and surface roughness. Specifically, the calibration showed i)
19
20 325 a positive correlation between surface roughness and soil moisture for dry conditions resulting in
21
22 326 small H_r values for dry soil, and ii) a negative trend for soil moisture values of $\sim 0.20 \text{ m}^3\text{m}^{-3}$ or
23
24 327 higher by decreasing the roughness effect with increasing moisture content. These findings also
25
26
27 328 agreed with the results published by [31] who investigated the impact of soil moisture on surface
28
29 329 roughness using single-angle NAFE'05 data. In that study the decrease of the roughness effect
30
31
32 330 for low soil moisture was associated with a reduced dielectric heterogeneity at micro-scale
33
34 331 during the drying process of the clay loam soils that dominate the study area. That is, the micro-
35
36 332 scale variability and thus the dielectric roughness would peak at intermediate soil moisture
37
38
39 333 content and decrease in very wet or very dry conditions. Hence, applying a reduced roughness
40
41 334 parameter from a non-linear function for dry conditions would ultimately produce better results
42
43
44 335 when comparing the forward simulations and the airborne measurements. The current SMOS
45
46 336 Level 2 soil moisture retrieval algorithms [23] include the sensitivity of surface roughness on soil
47
48 337 moisture in terms of a simple linear function such as that applied in this study. The roughness
49
50 338 estimation, however, is confined by the field capacity as an upper limit and a transition moisture
51
52
53 339 point as the lower limit, with both parameters being a function of the soil texture (sand/clay
54
55 340 content). Above and below these two points the roughness value is a constant, and the minimum
56
57
58
59
60

1
2
3 341 H_r value is expressed by $H_rMIN=(2k\sigma)^2$ [32], with k being the wave number and σ defined as the
4
5
6 342 surface root mean square height. Note, that i) the corresponding minimum and maximum H_r
7
8 343 values are dependent on the actual land cover type observed and ii) the maximum H_rMAX
9
10 344 parameter is retrieved from the individual SMOS scene.

11
12
13 345 The L-MEB parameterization of the third model included i) the moisture dependent roughness
14
15 346 factor H_r tested in the second model approach and ii) specifically calibrated vegetation structure
16
17 347 parameters tt_h and tt_v , that account for the angular dependency of the vegetation attenuation. The
18
19 348 corresponding forward model results showed the overall best agreement with the airborne data
20
21 349 (rmse=2.5-5.3 K) and the trend of the predicted dual-polarization curves captured that of the
22
23 350 measured data for both moist and dry soil moisture conditions. Compared to the default
24
25 351 parameterization and the high tt_v value of 8 obtained for the vertically dominated wheat canopy
26
27 352 [15], the vegetation structure parameters calibrated and tested in this study were significantly
28
29 353 lower and closer to unity (~ 1). Though it should be noted, that an individual calibration of the tt_p
30
31 354 parameters for each single day suggested a value of $tt_v = 3$ in one case, but overall only minor
32
33 355 variations across the different dates were observed. Consequently, the calibrated vegetation
34
35 356 structure parameters from the 9th of November 2005 were validated on different moisture
36
37 357 conditions and locations (Cullingral), confirming the good results obtained using this particular
38
39 358 parameterization. Further analysis showed that using the individually estimated tt_p values for
40
41 359 each observation day, instead of the values calibrated from the 9 November 2005, improved the
42
43 360 model rmse performance by 0.1 K at most. Moreover, the results demonstrated that the
44
45 361 adjustment of both angular correction parameters had a more significant impact on the predicted
46
47 362 brightness temperatures, when the ground measured vegetation water content was high (>1.9
48
49 363 kg/m^2) and thus, the attenuation effects of the canopy and its own contribution to the composite
50
51
52
53
54
55
56
57
58
59
60

1
2
3 364 brightness temperature increased as well. Consequently, both structure parameters play a major
4
5 365 role especially for large incidence angles ($> 30^\circ$) where the path length of the emitted energy
6
7
8 366 through the vegetation layer is longer.
9

10 367 The soil moisture retrieval based on an iterative least-squared algorithm resulted in a range of
11
12 368 soil moisture values depending on the model parameterizations chosen (Fig. 4). The default
13
14 369 parameterization generally produced too low soil moisture values with a maximum difference of
15
16 370 $\sim 0.3 \text{ m}^3\text{m}^{-3}$, if compared against the measured soil moisture. The overall best result with the
17
18 371 retrieved soil moisture being close ($\leq 0.04 \text{ m}^3\text{m}^{-3}$) to the observed moisture conditions was
19
20 372 achieved using the optimized set of parameters, which included the soil moisture dependent
21
22 373 roughness value H_r and the calibrated vegetation structure values tt_p (third model approach).
23
24
25
26
27

28 374 VI. CONCLUSION

29
30 375 This paper has presented simulations of brightness temperatures at a range of incidence angles
31
32 376 and the subsequent comparison with multi-incidence angle airborne observations over two wheat
33
34 377 canopy test sites in eastern Australia. The forward model used in this research was the L-band
35
36 378 Microwave Emission of the Biosphere (L-MEB) model which is one of the core elements of the
37
38 379 SMOS soil moisture retrieval algorithm. Apart from the default model parameterization proposed
39
40 380 by [15], two additional parameterizations were studied, including modifications of the surface
41
42 381 roughness and vegetation structure characterization. The performance of the individual model
43
44 382 approach was not only assessed based on changing moisture conditions, but also for different
45
46 383 locations in order to test its robustness. The agreement of the predicted and the measured
47
48 384 brightness temperature data from different the forward model parameterizations varied
49
50 385 significantly; with the observed discrepancy being much larger for wet conditions than for dry
51
52 386 soil moisture values. However, compared to the results using the default model parameterization,
53
54
55
56
57
58
59
60

1
2
3 387 a stepwise improvement was achieved by firstly introducing a soil moisture dependent roughness
4
5 388 factor and secondly by optimizing the vegetation structure parameters. Consequently, the dual-
6
7 389 polarized brightness temperature predictions were improved by minimizing the rmse from 38.1
8
9 390 K to 2.3 K for wet soil conditions ($\sim 0.45 \text{ m}^3 \text{ m}^{-3}$) and from 26.5 K to 5.3 K for dry soils (~ 0.13
10
11 $\text{m}^3 \text{ m}^{-3}$).
12
13 391 $\text{m}^3 \text{ m}^{-3}$).

14
15 392 This study proves that neglecting the sensitivity of the surface roughness parameter H_r on soil
16
17 393 moisture leads to a significant underestimation of the soil emission at L-band, which would
18
19 394 consequently affect the overall soil moisture retrieval accuracy. Furthermore, it was shown that
20
21 395 the transmissivity of a dominantly vertical canopy structure and the angular dependency of the
22
23 396 optical depth should not be neglected for vegetation water contents of $> 1.9 \text{ kg/m}^2$ and wet soil
24
25 397 conditions ($> 0.4 \text{ m}^3 \text{ m}^{-3}$), otherwise the error introduced into the retrieved soil moisture product
26
27 398 for the given data set could be up to $0.3 \text{ m}^3 \text{ m}^{-3}$. Though it should be noted that considering the
28
29 399 spatial resolution of SMOS observations and a footprint size of approximately $\sim 42 \text{ km}$, which
30
31 400 captures a mixture of land cover types, the angular effect is likely to be minor for SMOS
32
33 401 products. However, this issue needs to be investigated in future research to understand the impact
34
35 402 of the angular vegetation structure effects on the soil moisture retrieval at satellite scale. Based
36
37 403 on the demonstrated results, the effect of dominantly vertically structured canopies should be
38
39 404 assessed by comparing the single-angle and multi-angle soil moisture retrieval performance
40
41 405 using both passive microwave data from airborne observations and SMOS.
42
43
44
45
46
47
48

49 VII. ACKNOWLEDGMENT

50
51
52 407 The authors would like to thank the NAFE'05 team for collecting and providing the data set
53
54 408 used in this study. This work was supported by the Australian Research Council (DP0879212)
55
56 409 within the framework of the Moisture Map project.
57
58
59
60

410

411

REFERENCES

- [1] T. J. Schmugge, P. E. O'Neill, and J. R. Wang, "Passive microwave soil moisture research," *IEEE Trans. Geosci. Remote Sens.*, vol. GE-24, no. 1, pp. 12-22, 1986.
- [2] J. C. Calvet, J. P. Wigneron, A. Chanzy, and D. Haboudane, "Retrieval of surface parameters from microwave radiometry over open canopies at high frequencies," *Remote Sens. Environ.*, vol. 53, pp. 46-60, 1995.
- [3] T. J. Jackson, J. Schmugge, and E. T. Engman, "Remote sensing applications to hydrology: Soil moisture," *Hydrol. Sci. J.*, vol. 41, no. 4, pp. 517-530, 1996.
- [4] E. G. Njoku and D. Entekhabi, "Passive microwave remote sensing of soil moisture," *J. Hydrol.*, vol. 184, no. 1-2, pp. 101-129, 1996.
- [5] C. Pathe, W. Wagner, D. Sabel, M. Doubkova, and J. B. Basara, "Using ENVISAT ASAR Global Mode Data for Surface Soil Moisture Retrieval Over Oklahoma, USA," *IEEE Trans. Geosci. Remote Sens.*, vol. 47, pp. 468-480, 2009.
- [6] C. Rüdiger, J.-C. Calvet, C. Gruhier, T. R. H. Holmes, R. A. M. de Jeu, and W. Wagner, "An Intercomparison of ERS-Scat and AMSR-E Soil Moisture Observations with Model Simulations over France," *J. Hydrometeorol.*, vol. 10, pp. 431-447, 2009.
- [7] J. Wigneron, J. Calvet, T. Pellarin, A. Van de Griend, M. Berger, and P. Ferrazzoli, "Retrieving near-surface soil moisture from microwave radiometric observations: current status and future plans," *Remote Sens. Environ.*, vol. 85, no. 4, pp. 489-506, 2003.
- [8] J. Leese, T. Jackson, A. Pitman, and P. Dirmeyer, "GEWEX/BAHC International workshop on soil moisture monitoring, analysis, and prediction for hydrometeorological and hydroclimatological applications," *Bulletin of the American Meteorological Society*, vol. 82, pp. 1423-1430, 2001.
- [9] Y. Kerr, P. Waldteufel, J. P. Wigneron, J. M. Martinuzzi, J. Font and M. Berger, "Soil moisture retrieval from space: The Soil Moisture and Ocean Salinity (SMOS) mission," *IEEE Trans. Geosci. Remote Sens.* vol. 39, no. 8: pp. 1729-1735, Aug. 2001.
- [10] Y. Kerr, P. Waldteufel, J. Wigneron, S. Delwart, F. Cabot, J. Boutin, M. Escorihuela, J. Font, N. Reul, and C. Gruhier, "The SMOS Mission: New Tool for Monitoring Key Elements of the Global Water Cycle," *Proceedings of the IEEE*, vol. 98, pp. 666-687, 2010.

- 1
2
3
4 440 [11]M. Pardé, J. P. Wigneron, A. Chanzy, P. Waldteufel, Y. Kerr, and S. Huet, "Retrieving
5 441 surface soil moisture over a wheat field: comparison of different methods," *Remote Sens.*
6
7 442 *Environ.*, vol. 87, pp. 334-344, 2003.
- 8
9 443 [12]M. J. Sandells, I. J. Davenport, and R. J. Gurney, "Passive L-band microwave soil moisture
10 444 retrieval error arising from topography in otherwise uniform scenes," *Adv. Water Resour.*,
11
12 445 vol. 31, pp. 1433-1443, 2008.
- 13
14 446 [13]J. Wigneron, M. Parde, P. Waldteufel, A. Chanzy, Y. Kerr, S. Schmidl, and N. Skou,
15
16 447 "Characterizing the dependence of vegetation model parameters on crop structure, incidence
17 448 angle, and polarization at L-band," *IEEE Trans. Geosci. Remote Sens.*, vol. 42, pp. 416-425,
18
19 449 Feb. 2004.
- 20
21 450 [14]J. Wigneron, P. Waldteufel, A. Chanzy, J. Calvet, and Y. Kerr, "Two-dimensional
22 451 microwave interferometer retrieval capabilities over land surfaces(SMOS Mission)," *Remote*
23
24 452 *Sens. Environ.*, vol. 73, pp. 270-282, 2000.
- 25
26 453 [15]J. Wigneron, Y. Kerr, P. Waldteufel, K. Saleh, M. Escorihuela, P. Richaume, P. Ferrazzoli,
27
28 454 P. de Rosnay, R. Gurney, and J. Calvet, "L-band Microwave Emission of the Biosphere (L-
29
30 455 MEB) Model: Description and calibration against experimental data sets over crop fields,"
31
32 456 *Remote Sens. Environ.*, vol. 107, pp. 639-655, Apr. 2007.
- 33
34 457 [16]I. Davenport, J. Fernandez-Galvez, and R. Gurney, "A sensitivity analysis of soil moisture
35 458 retrieval from the tau-omega microwave emission model," *IEEE Trans. Geosci. Remote*
36
37 459 *Sens.*, vol. 43, pp. 1304-1316, 2005.
- 38
39 460 [17]P. de Rosnay, J. Calvet, Y. Kerr, J. Wigneron, F. Lemaître, M. Escorihuela, J. Sabater, K.
40
41 461 Saleh, J. Barrié, and G. Bouhours, "SMOSREX: A long term field campaign experiment for
42 462 soil moisture and land surface processes remote sensing," *Remote Sens. Environ.*, vol. 102,
43
44 463 pp. 377-389, 2006.
- 45
46 464 [18]A. Cano, K. Saleh, J.-P. Wigneron, C. Antolín, J. E. Balling, Y. H. Kerr, A. Kruszewski, C.
47
48 465 Millán-Scheiding, S. S. Søbjaerg, N. Skou, and E. López-Baeza, "The SMOS Mediterranean
49
50 466 Ecosystem L-Band characterisation EXperiment (MELBEX-I) over natural shrubs," *Remote*
51
52 467 *Sens. Environ.*, vol. 114, pp. 844-853, 2010.
- 53
54 468 [19]K. Saleh, J. Wigneron, J. Calvet, E. Lopez-Baeza, P. Ferrazzoli, M. Berger, P. Wursteisen,
55
56 469 L. Simmonds, and J. Miller, "The EuroSTARRS airborne campaign in support of the SMOS
57 470 mission: first results over land surfaces," *J. Remote Sens.*, vol. 25, pp. 177-194, 2004.
- 58
59
60

- 1
2
3 471 [20]R. Panciera, J. P. Walker, J. D. Kalma, E. J. Kim, J. M. Hacker, O. Merlin, M. Berger, and
4
5 472 N. Skou, "The NAFE'05/CoSMOS Data Set: Toward SMOS Soil Moisture Retrieval,
6
7 473 Downscaling, and Assimilation," *IEEE Trans. Geosci. Remote Sens.*, vol. 46, pp. 736-745,
8
9 474 Mar. 2008.
- 10 475 [21]C. Rüdiger, G. Hancock, H. M. Hemakumara, B. Jacobs, J. D. Kalma, C. Martinez, M.
11
12 476 Thyer, J. P. Walker, T. Wells, and G. R. Willgoose, "Goulburn River experimental catchment
13
14 477 data set," *Water Resour. Res.*, vol. 43, p. W10403, 2007.
- 15 478 [22]O. Merlin, J. Walker, R. Panciera, R. Young, J. Kalma, and E. Kim, "Soil moisture
16
17 479 measurement in heterogeneous terrain," *MODelling and SIMulation Society of Australia and*
18
19 480 *New Zealand. New Zealand*, 2007.
- 20 481 [23]Y. Kerr, P. Waldteufel, P. Richaume, P. Ferrazzoli, and J. Wigneron, "SMOS level 2
21
22 482 Processor for Soil Moisture Algorithm Theoretical Based Document (ATBD)," CESBIO,
23
24 483 Toulouse, SO-TN-ESL-SM-GS-0001, v3.a., Oct. 15, 2008.
- 25 484 [24]T. J. Jackson and T. J. Schmugge, "Vegetation effects on the microwave emission of soils,"
26
27 485 *Remote Sens. Environ.*, vol. 36, pp. 203-212, 1991.
- 28 486 [25]J. Wigneron, A. Chanzy, J. Calvet, and N. Bruguier, "A simple algorithm to retrieve soil
29
30 487 moisture and vegetation biomass using passive microwave measurements over crop fields,"
31
32 488 *Remote Sens. Environ.*, vol. 51, pp. 331-341, Aug. 1995.
- 33 489 [26]R. Panciera, J. Walker, J. Kalma, E. Kim, K. Saleh, and J. Wigneron, "Evaluation of the
34
35 490 SMOS L-MEB passive microwave soil moisture retrieval algorithm," *Remote Sens. Environ.*,
36
37 491 vol. 113, pp. 435-444, Feb. 2009.
- 38 492 [27]J. Wigneron, L. Laguerre, and Y. Kerr, "A simple parameterization of the L-band microwave
39
40 493 emission from rough agricultural soils," *IEEE Trans. Geosci. Remote Sens.*, vol. 39, pp.
41
42 494 1697-1707, Aug. 2001.
- 43 495 [28]T. Mo and T. Schmugge, "A parameterization of the effect of surface roughness on
44
45 496 microwave emission," *IEEE Trans. Geosci. Remote Sens.*, vol. 25, pp. 47-54, Jan. 1987.
- 46 497 [29]K. Saleh, Y. H. Kerr, P. Richaume, M. J. Escorihuela, R. Panciera, S. Delwart, G. Boulet, P.
47
48 498 Maisongrande, J. P. Walker, and P. Wursteisen, "Soil moisture retrievals at L-band using a
49
50 499 two-step inversion approach (COSMOS/NAFE'05 Experiment)," *Remote Sens. Environ.*, vol.
51
52 500 113, pp. 1304-1312 2009.
53
54
55
56
57
58
59
60

- 1
2
3 501 [30]M. Escorihuela, Y. Kerr, P. de Rosnay, J. Wigneron, J. Calvet, and F. Lemaitre, "A Simple
4
5 502 Model of the Bare Soil Microwave Emission at L-Band," *IEEE Trans. Geosci. Remote Sens.*,
6
7 503 vol. 45, pp. 1978-1987, 2007.
- 8
9 504 [31]R. Panciera, J. Walker, and O. Merlin, "Improved Understanding of Soil Surface Roughness
10
11 505 Parameterization for L-Band Passive Microwave Soil Moisture Retrieval," *IEEE Trans.*
12
13 506 *Geosci. Remote Sens. Lett.*, vol. 6, pp. 625-629, Oct. 2009.
- 14 507 [32]B. Choudhury, T. J. Schmugge, A. Chang, and R. Newton, "Effect of surface roughness on
15
16 508 the microwave emission from soils," *J. Geophysical Res.*, vol. 84, pp. 5699-5706, 1979

17
18 509
19 510

For Peer Review

20
21
22
23
24
25
26
27
28
29
30
31
32
33
34
35
36
37
38
39
40
41
42
43
44
45
46
47
48
49
50
51
52
53
54
55
56
57
58
59
60

511

TABLES

TABLE I: Characteristics of selected NAFE'05 focus farms with multi-incidence angle observations

TABLE II: Parameterization of the three forward models studied

FIGURES

Fig. 1. Locations of NAFE'05 Focus farms, multi-angle flight lines, soil moisture measurements and monitoring stations in the Goulburn River catchment, New South Wales, Australia.

Fig. 2. Dual-polarized brightness temperature estimates plotted against incidence angle and compared to multi-angle PLMR observations over wheat canopy available for Merriwa Park and Cullingral. The forward simulations were based on three different model parameterization (default, Hr-cal, optimized) as given in Table II. Note, that only the data from 9 Nov 2005 at Merriwa Park were used for model calibration (optimized model), whereas the remaining datasets were used for validation purpose.

Fig. 3. Scatterplot of the L-MEB model simulations in comparison with independent ground data from Merriwa Park at different observation dates using the default model parameterization (dots) [15], the site-specific roughness parameterization (crosses) [26] and the optimized model parameterization (circles). The root mean square errors [K] are given for all model approaches.

Fig. 4. Scatterplot showing the retrieved against the measured soil moisture values at the Merriwa Park focus farm for the four available observation days. The inverse application of the L-MEB model was made for all three model parameterizations discussed in Section IV.

TABLE I
CHARACTERISTICS OF SELECTED NAFE'05 FOCUS FARMS WITH MULTI-INCIDENCE ANGLE OBSERVATIONS

SITE	OBSERVATIONS DAYS	LAND COVER	TOPOGRAPHY	SOIL TYPE	SAND CONTENT [%]	CLAY CONTENT [%]	VEGETATION	SOIL MOISTURE ^a
							WATER CONTENT ^a MIN-MAX [kg/m ²]	MIN-MAX [m ³ /m ³]
Merriwa Park	4	Native grass + agriculture (wheat)	Gently sloping	Silt clay loam	21	30	0.70 - 3.00	0.10 – 0.50
Cullingral	1	Native grass + agriculture (wheat/barley)	Flat	Silty loam	36	26	0.14 – 0.47	0.03 – 0.09

^aacross area with wheat cover

TABLE II
PARAMETERIZATION OF THE THREE FORWARD MODELS STUDIED

MODEL	ROUGHNESS				VEGETATION				COMMENT
	H_r	N_{rh}	N_{rv}	tt_h	tt_v	ω_h	ω_v		
Default	0.1	0	0	1	8	0	0	Parameterization proposed by [15]	
Hr-cal	1.5-1.6-SM ^a ** 1.6-1.0-SM ^a ***	0	0	1	8	0	0	Soil moisture dependent H_r component [26]	
Optimized	1.5-1.6-SM ^a ** 1.6-1.0-SM ^a ***	0	0	0.2	1.4	0	0	Soil moisture dependent H_r [26] and optimized vegetation structure values calibrated from multi-incidence angle data from Merriwa Park 09/11/2005	

^aSM: Soil Moisture; *Roughness function for Merriwa Park; **Roughness function for Cullingral

Peer Review

1
2
3
4
5
6
7
8
9
10
11
12
13
14
15
16
17
18
19
20
21
22
23
24
25
26
27
28
29
30
31
32
33
34
35
36
37
38
39
40
41
42
43
44
45
46
47
48
49
50
51
52
53
54
55
56
57
58
59
60

1
2
3
4
5
6
7
8
9
10
11
12
13
14
15
16
17
18
19
20
21
22
23
24
25
26
27
28
29
30
31
32
33
34
35
36
37
38
39
40
41
42
43
44
45
46
47
48
49
50
51
52
53
54
55
56
57
58
59
60

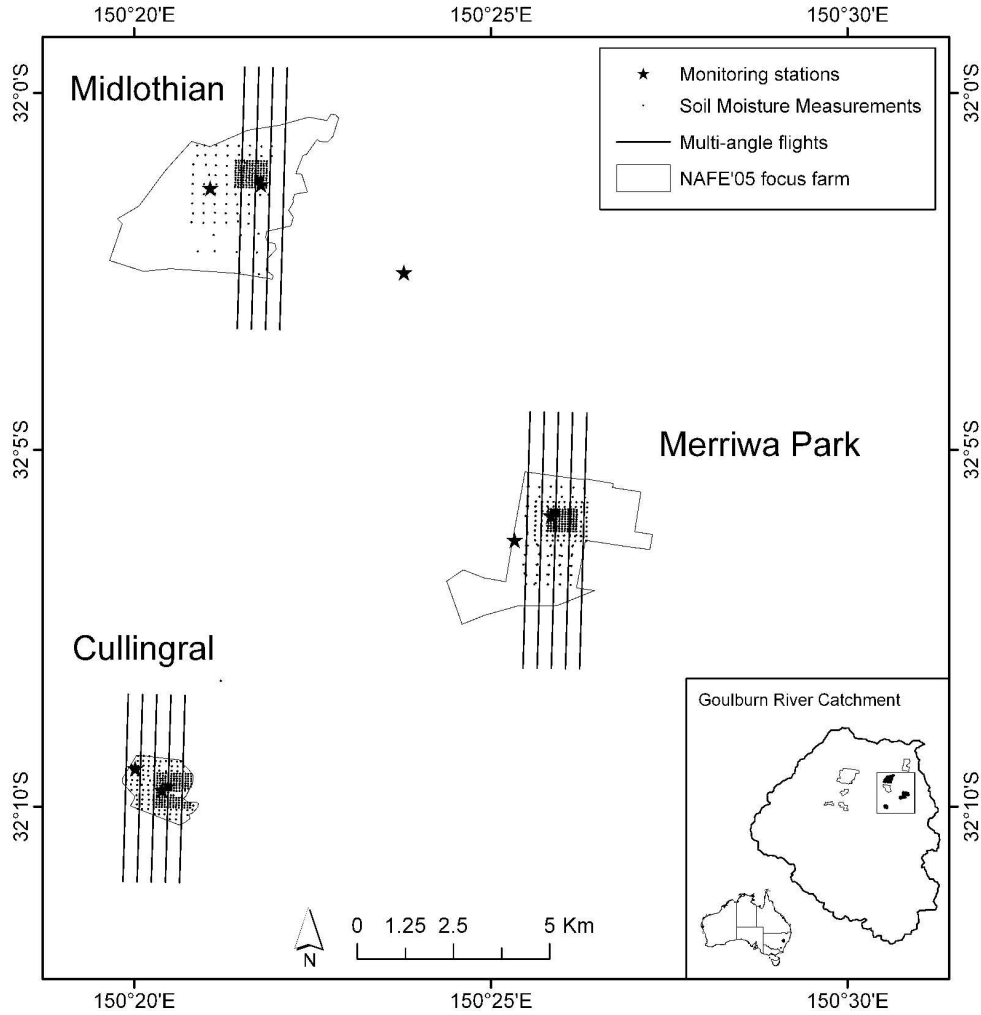


Fig. 1. Locations of NAFE'05 Focus farms, multi-angle flight lines, soil moisture measurements and monitoring stations in the Goulburn River catchment, New South Wales, Australia. 206x212mm (600 x 600 DPI)

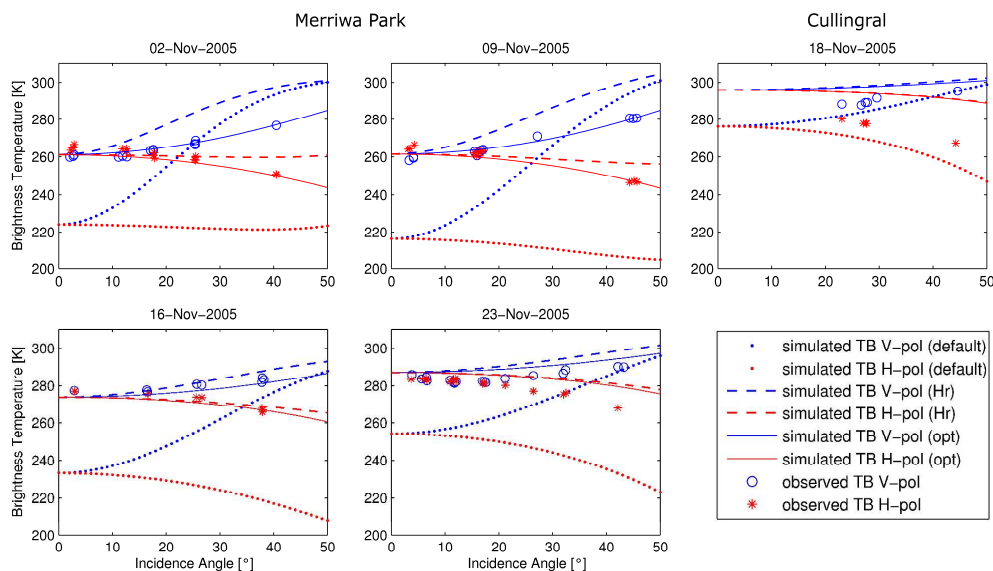


Fig. 2. Dual-polarized brightness temperature estimates plotted against incidence angle and compared to multi-angle PLMR observations over wheat canopy available for Merriwa Park and Cullingral. The forward simulations were based on three different model parameterization (default, Hr-cal, optimized) as given in Table II. Note, that only the data from 9 Nov 2005 at Merriwa Park were used for model calibration (optimized model), whereas the remaining datasets were used for validation purpose.

253x145mm (600 x 600 DPI)

Review

1
2
3
4
5
6
7
8
9
10
11
12
13
14
15
16
17
18
19
20
21
22
23
24
25
26
27
28
29
30
31
32
33
34
35
36
37
38
39
40
41
42
43
44
45
46
47
48
49
50
51
52
53
54
55
56
57
58
59
60

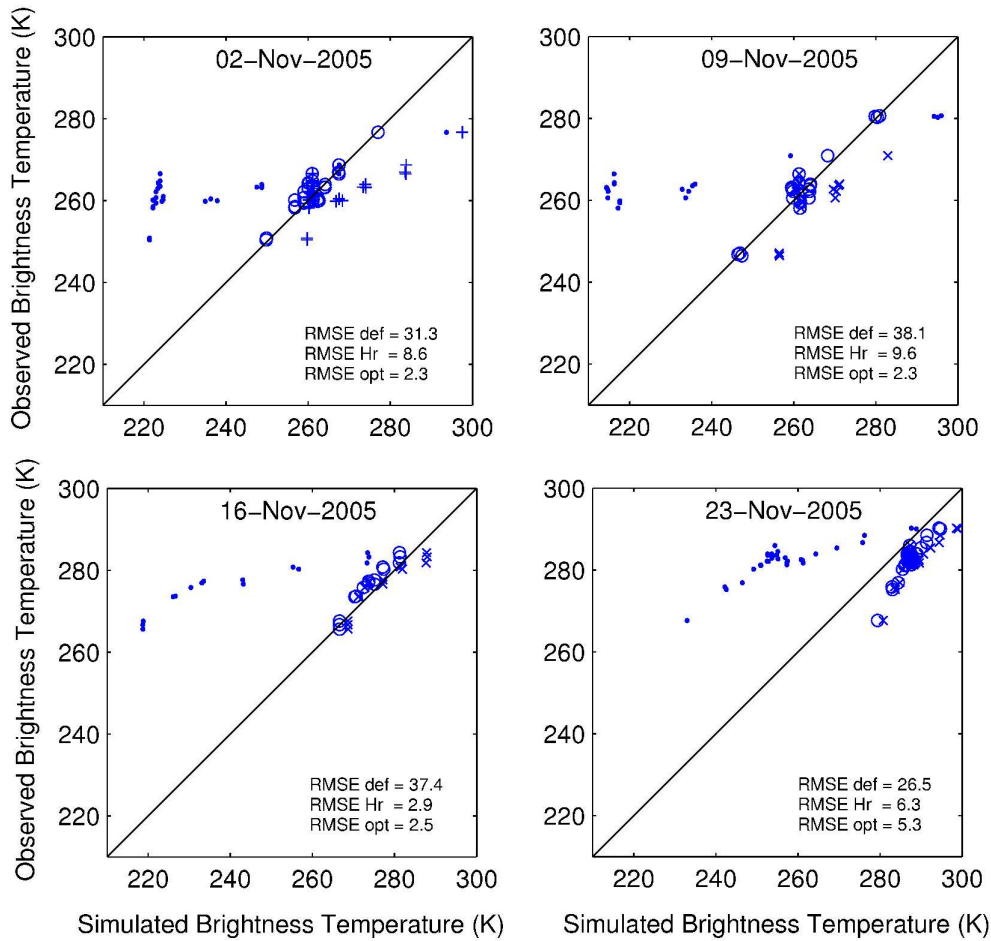


Fig. 3. Scatterplot of the L-MEB model simulations in comparison with independent ground data from Merriwa Park at different observation dates using the default model parameterization (dots) [15], the site-specific roughness parameterization (crosses) [26] and the optimized model parameterization (circles). The root mean square errors [K] are given for all model approaches. 141x134mm (600 x 600 DPI)

1
2
3
4
5
6
7
8
9
10
11
12
13
14
15
16
17
18
19
20
21
22
23
24
25
26
27
28
29
30
31
32
33
34
35
36
37
38
39
40
41
42
43
44
45
46
47
48
49
50
51
52
53
54
55
56
57
58
59
60

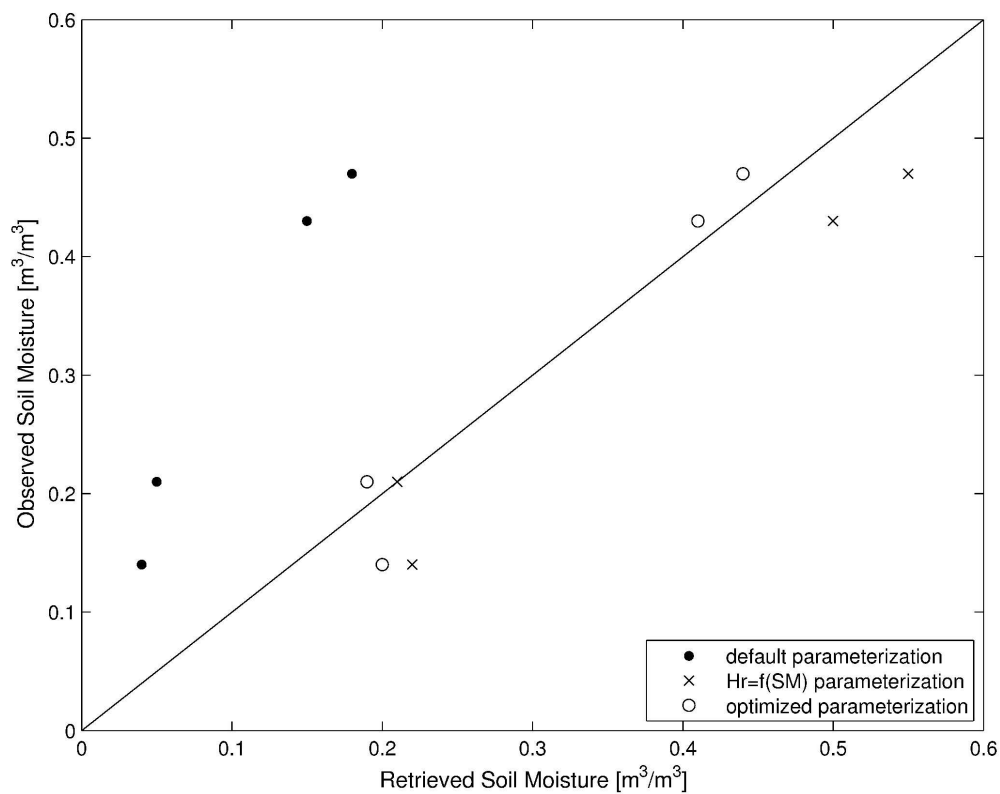


Fig. 4. Scatterplot showing the retrieved against the measured soil moisture values at the Merriwa Park focus farm for the four available observation days. The inverse application of the L-MEB model was made for all three model parameterizations discussed in Section IV.
174x140mm (600 x 600 DPI)